

## Supplementary materials : Orientational dynamics in supercooled glycerol computed from MD simulations: self and cross contributions

Marceau Hénot,<sup>1,\*</sup> Pierre-Michel Déjardin,<sup>2</sup> and François Ladieu<sup>1</sup>

<sup>1</sup>*SPEC, CEA, CNRS, Université Paris-Saclay, CEA Saclay Bat 772, 91191 Gif-sur-Yvette Cedex, France.*

<sup>2</sup>*Laboratoire de Modélisation Pluridisciplinaire et Simulations, Université de Perpignan Via Domitia, 52 avenue Paul Alduy, F-66860 Perpignan, France.*

(Dated: 11th October 2023)

### I. FORCE FIELD FOR GLYCEROL

The force field used in this work is the one initially introduced by Chelli *et al.* [1, 2], later optimized by Blicek *et al.* [3] and used since with only little differences by Egorov *et al.* [4], Busselez *et al.* [5] and Becher *et al.* [6]. The partial charges used for the glycerol molecules are shown in fig. S5. The harmonic bond, harmonic angle, and periodic torsion forces parameters are given in table S1, S2 and S3 respectively. The Lennard-Jones parameters are given in table S4.

### II. SIMULATION RUNS

The simulation runs used in this work are described in table S5. At each temperature  $T < 323$  K, the equilibration is performed starting from the equilibrated state at  $T + 10$  K.

### III. EFFECT OF THE SIMULATION BOX SIZE

The effect of the simulation box size was studied by performing an additional simulation run at 323 K for only  $N = 540$  molecules (7560 atoms) in a cubic cell of side length  $a \approx 41$  Å. The dipole density  $n(r)$  and the integrated cross-correlation contribution  $\int_0^r c_1(r', t = 0) dr$  are shown in fig. S1 for this case as well as for the box size used in the main text ( $N = 2160$ ,  $a \approx 65$  Å) at the same temperature. Both datasets display a similar behavior regarding cross-correlations: a first plateau is reached at  $r \approx 8$  Å followed by an increase with a maximum slope reached at  $r = a/2$ . This box-size dependent second regime is due to the effect of PBCs on the treatment of electrostatic interactions with the PME method [7–9]. Using  $N = 2160$  allows us to safely decouple the PCBs artifact from the physically meaningful behavior at  $r < 15$  Å.

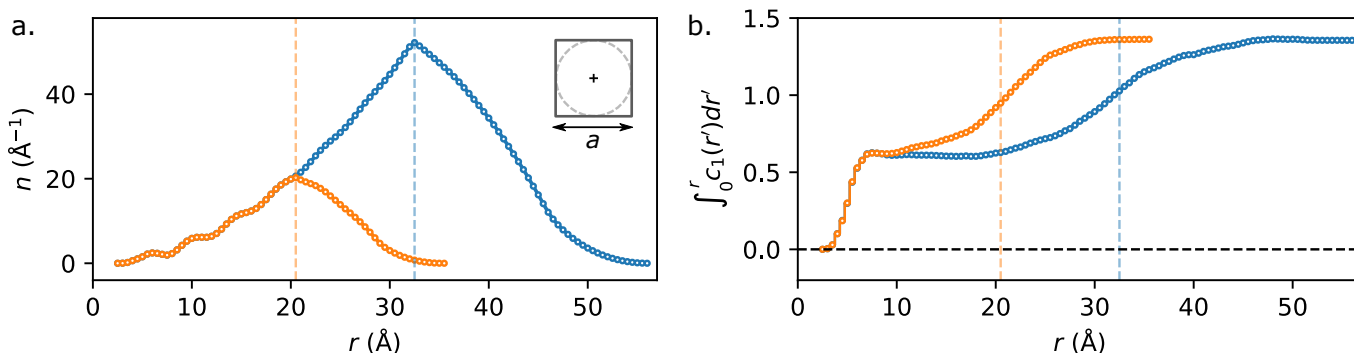


Figure S1. Effect of the simulation box size at  $T = 323$  K  $N = 2160$  molecules used in this study (blue) and  $N = 540$  (orange). (a) Dipole density  $n(r)$ . The vertical dashed lines correspond to the half side  $a/2$  of the simulation box. (b) Integrated cross-correlation  $\int_0^r c_1(r', t = 0) dr$ .

\* Corresponding author: marceau.henot@cea.fr

Table S1. Harmonic bond force parameters. The potential is of the form  $E_b = k_b(r - r_0)^2$ .

bond	$k_b$ (kcal·mol <sup>-1</sup> ·Å <sup>-2</sup> )	$r_0$ (Å)
CC	310	1.526
CO	320	1.410
CH	rigid bond	1.090
OH	rigid bond	0.960

#### IV. CORRELATION FUNCTION

The correlation functions shown in fig. 1 and 4 of the main text are reproduced in fig. S2 and S2 with a logarithmic vertical axis in order to make the long time behaviour more visible.

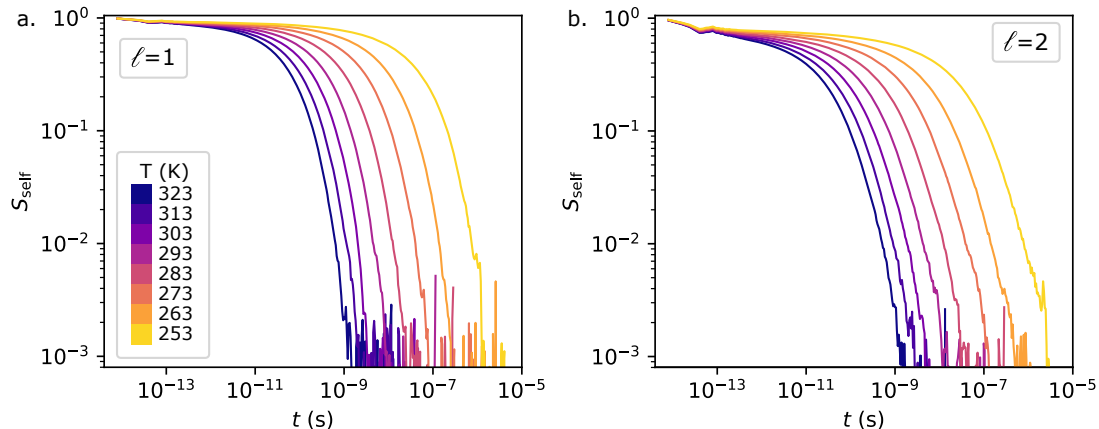
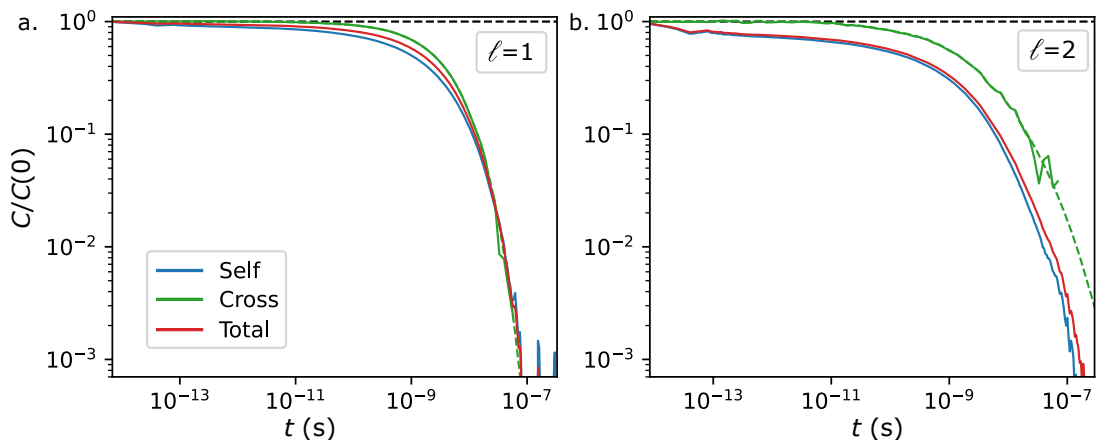


Figure S2. Dipole self correlation function (from fig. 1a of the main text) plotted with a logarithmic vertical axis.

Figure S3. Correlation functions at  $T = 273$  K (from fig. 4a-b of the main text) plotted with a logarithmic vertical axis. The dashed green line is an exponential fit on the long time part of the cross correlation function used to obtain the total correlation function  $S_{\text{tot}} = S_{\text{self}} + S_{\text{cross}}$ .

#### V. COMPARISON OF $\mu^2 g_K$ WITH EXPERIMENTS

Fig. S4 shows  $\mu^2 g_K$  obtained from the MD simulation in this work (red) and from experimental measurements of  $\epsilon(0)$  and eq. 1 of the main text by Gabriel *et al.* [10].

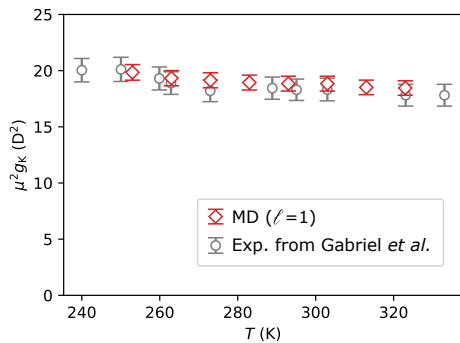


Figure S4. Temperature dependence of  $\mu^2 g_K$  obtained from the MD simulation and experimentally from the measurement of the dielectric strength (from ref. [10]).

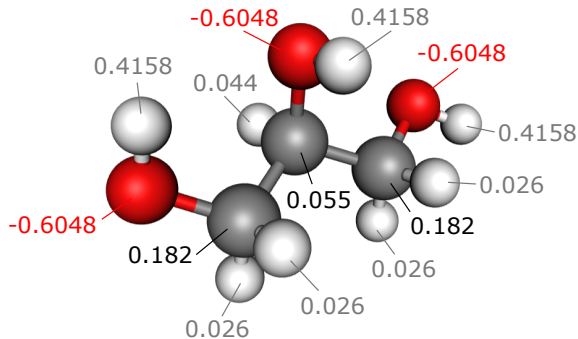


Figure S5. Atomic charges of the glycerol molecule.

Table S2. Harmonic angle force parameters. The potential is of the form  $E_\theta = k_\theta(\theta - \theta_0)^2$ .

angle	$k_\theta$ (kcal·mol <sup>-1</sup> ·rad <sup>-2</sup> )	$\theta_0$ (°)
CCC	40	109.5
CCO	50	109.5
CCH	50	109.5
COH	55	108.5
HCH	35	109.5
OCH	50	109.5

Table S3. Periodic torsion force parameters. The potential is of the form  $E_\Phi = k_\Phi(1 + \cos(n\Phi))$ .

dihedral	$V_n$ (kcal·mol <sup>-1</sup> )	$n$
CCCH	0.1556	3
CCCO	0.1556	3
OCCO	0.1440	3
OCCO	1.0000	2
OCCH	0.1556	3
HOCC	0.1667	3
HOCH	0.1667	3
HCCH	0.1556	3

Table S4. Lennard-Jones parameters. The potential is of the form  $V_{LJ} = 4 \left( \left( \frac{\sigma}{r} \right)^{12} - \left( \frac{\sigma}{r} \right)^6 \right)$ . The input parameters of the Amber .frcmod file is the half atom-atom distance at which the potential reaches its minimum ( $R_m = 2^{1/6}\sigma$ ).

atom	$R_m/2$ (Å)	$\sigma$ (Å)	$\epsilon$ (kcal·mol <sup>-1</sup> )
C	2.1416	3.816	0.1094
O	1.6000	2.850	0.1591
aliphatic H	1.5569	2.774	0.0157
hydroxyl H	0.800	1.425	0.0498

Table S5. Details on the simulation runs.

$T$ (K)	equil. steps	in $\tau_{\text{self}}$ unit.	in s	run steps	in $\tau_{\text{self}}$ unit.	in s
323	$4 \times 10^6$	213	16 ns	$3.5 \times 10^6$	186	14 ns
313	$7 \times 10^6$	225	28 ns	$7 \times 10^6$	225	28 ns
303	$14 \times 10^6$	253	56 ns	$14 \times 10^6$	253	56 ns
293	$33 \times 10^6$	262	130 ns	$30 \times 10^6$	238	120 ns
283	$38 \times 10^6$	114	150 ns	$75 \times 10^6$	225	300 ns
273	$108 \times 10^6$	113	430 ns	$215 \times 10^6$	226	430 ns
263	$358 \times 10^6$	98	1.4 $\mu\text{s}$	$710 \times 10^6$	194	2.8 $\mu\text{s}$
253	$1830 \times 10^6$	101	7.3 $\mu\text{s}$	$1210 \times 10^6$	67	4.8 $\mu\text{s}$

- 
- [1] R. Chelli, P. Procacci, G. Cardini, R. G. Della Valle, and S. Califano, Glycerol condensed phases part i. a molecular dynamics study, *Physical Chemistry Chemical Physics* **1**, 871 (1999).
  - [2] R. Chelli, Glycerol condensed phases. Part II. A molecular dynamics study of the conformational structure and hydrogen bonding, *Physical Chemistry Chemical Physics* **1**, 879 (1999).
  - [3] J. Blicek, F. Affouard, P. Bordat, A. Lerbret, and M. Descamps, Molecular dynamics simulations of glycerol glass-forming liquid, *Chemical Physics* , 5 (2005).
  - [4] A. V. Egorov, A. P. Lyubartsev, and A. Laaksonen, Molecular Dynamics Simulation Study of Glycerol–Water Liquid Mixtures, *The Journal of Physical Chemistry B* **115**, 14572 (2011).
  - [5] R. Busselez, T. Pezeril, and V. E. Gusev, Structural heterogeneities at the origin of acoustic and transport anomalies in glycerol glass-former, *The Journal of Chemical Physics* **140** (2014).
  - [6] M. Becher, T. Wohlfromm, E. Rössler, and M. Vogel, Molecular dynamics simulations vs field-cycling nmr relaxometry: Structural relaxation mechanisms in the glass-former glycerol revisited, *The Journal of Chemical Physics* **154**, 124503 (2021).
  - [7] J. Caillol, Asymptotic behavior of the pair-correlation function of a polar liquid, *The Journal of chemical physics* **96**, 7039 (1992).
  - [8] C. Zhang and M. Sprik, Computing the dielectric constant of liquid water at constant dielectric displacement, *Physical Review B* **93**, 144201 (2016).
  - [9] J.-F. Olivieri, J. T. Hynes, and D. Laage, Confined water’s dielectric constant reduction is due to the surrounding low dielectric media and not to interfacial molecular ordering, *The Journal of Physical Chemistry Letters* **12**, 4319 (2021).
  - [10] J. P. Gabriel, P. Zourchang, F. Pabst, A. Helbling, P. Weigl, T. Böhmer, and T. Blochowicz, Intermolecular cross-correlations in the dielectric response of glycerol, *Physical Chemistry Chemical Physics* **22**, 11644 (2020).